Universiteit Leiden
The Netherlands

In search of synergy: novel therapy for metastatic uveal melanoma
Glinkina, K.A.

Chapter

——————

5

COMPARATIVE PHOSPHOPROTEOME ANALYSIS OF PRIMARY AND METASTATIC UVEAL MELANOMA CELL LINES

Kseniya Glinkina[1], Roman Gonzalez Prieto[1], Amina F.A.S. Teunisse[1], Maria Chiara Gelmi[2], Martine J. Jager[2], Alfred.C.O. Vertegaal[1], Aart G. Jochemsen[1]

1. Department of Cell and Chemical Biology, Leiden University Medical Center, Leiden, The Netherlands
2. Department of Ophthalmology, Leiden University Medical Center, Leiden, The Netherlands

Abstract

Uveal melanoma (UM) is an ocular tumor that often develops asymptomatically. Statistically, every second patient eventually develops metastases that drastically worsen the prognosis by several months of overall survival. While isolated liver perfusion with melphalan and more recently immunotherapy (Tebentafusp) are the few treatment options available for metastatic UM patients, their application is complex or expensive. There is an urgent need to understand drug response and identify potential avenues for therapy. Hence, we focused on uncovering altered phosphorylation signaling events in metastatic UM using proteomics as an approach to identify potential drug targets.

We analyzed the phosphoproteomes of the primary UM cell line Mel270 and two cell lines OMM2.3 and OMM2.5, derived from metastatic lesions of the same patient. We found 177 phosphosites to be altered significantly between primary and metastatic cell lines. Pathway analysis of up-regulated phosphosites in metastatic lines suggests that Rho signaling and mitotic cell cycle to be significantly altered uncovering potential routes of signaling for metastasis. Clinical data from LUMC and TCGA datasets uncovered MARK3 expression (which links to Rho signaling) correlation with chromosome 3 status, a prognostic marker in UM, suggesting that MARK3 kinase might be involved in metastatic UM signaling.

Introduction

Uveal melanoma (UM) is a rare tumor originating from the melanocytes located in uveal tract of the eye. In many cases UM develops asymptomatically and metastasizes by the time of the diagnosis [1]. Spread of UM metastases affects up to 50% of the patients and drastically worsen the prognosis due to resistance of the metastatic lesions to commonly used therapeutics [2]. Several therapeutic options available for metastatic UM patients include isolated liver perfusion with melphalan and recently developed immunotherapy approach (Tebentafusp) [3-4]. However, these treatment options are suitable only for subsets of patients, are complex or expensive. Therefore, there is an urgent need to understand drug response and identify novel avenues for therapy.

The genetic profile of UM is distinct from one of cutaneous melanoma. UM lacks the mutations in BRAF and NRAS, common for cutaneous melanoma; instead, virtually all UM cases are characterized by activation of Gα-proteins signaling cascade. In more than 90% of UM cases the mutations are harbored in *GNAQ* and *GNA11* genes, encoding Gαq and Gα11 subunits respectively; the remaining cases are characterized by the activating mutations in G-protein coupled receptor *CYSLTR2* or in signal mediator *PLCB4* [5-7]. The persistent activity of the Gα-proteins signaling cascade dysregulates several downstream pathways [8-10]. It fuels in activity of RhoA and downstream effectors, which trigger translocation to nucleous of YAP1 and TAZ, start YAP1-dependent transcription and initiation of malignant transformation of uveal melanocytes [11-14].

Secondary somatic alterations most commonly occur in the genes *EIF1AX*, *SF3B1*, *BAP1* in a mutually exclusive manner [15-17]. The presence of inactivating mutations in the translation initiation factor EIF1AX correlates with disomy of chromosome 3 and more favorable prognosis, while inactivation of splicing modulator SF3B1 is associated with intermediate metastatic risk and late-onset metastases. Inactivating mutation in *BAP1* gene followed by loss of chromosome 3 leads to complete depletion of BAP1 expression and strongly correlates with metastases development and poor prognosis. Besides the somatic mutations, copy number alterations on the chromosomes 1q, 3, 6p, 6q, 8q, 16q are common in metastatic UM [18-20].

Despite recent progress in unraveling the genetic mechanisms of UM, limited studies are available examining the (phospho)proteome of primary UM and metastatic UM [21, 22]. In this study we analyzed the phosphoproteome of the primary UM cell line Mel270 and the cell lines OMM2.3 and OMM2.5, derived from metastatic lesions of the same patient. We found 177 differentially phosphorylated sites between primary tumor and metastases, identified up- and down-regulated signaling cascades in metastases and suggested that MARK3 kinase might be involved in YAP1/TAZ signaling regulation.

5

Results

Phosphoproteome analysis of primary and metastatic UM cell lines

To identify the signaling cascades involved in UM metastasis, we performed phosphoproteomics of a primary tumor-derived cell line (Mel270) and two other lines (OMM2.3 and OMM2.5) derived from UM hepatic metastases in quadruplicates. These three cell lines originate from the same individual, share a Q209P mutation in GNAQ, and harbor no mutations in BAP1, EIF1AX or SF3B1. Chromosome analysis of the Mel270 and OMM2.3 lines showed disomy of chromosome 3, tetrasomy of 6p and extra chromosomes 8 [29].

In total, we obtained intensities for 14,315 phosphosites and following stringent quality control step, we quantified 4,367 phosphosites in total. The phosphorylated amino acids were distributed as follows: 3,969 (90.8%) pS, 384 (8.9%) pT and 14 (0.3%) pY. The distribution of phosphorylation multiplicity showed that 2340 (53.6%), 1879 (43%) and 148 (3.4%) sites were phosphorylated at single, double, or multiple sites, respectively. The hierarchical clustering of these 4,367 phosphosites displayed greater separation between primary cell line and the two metastatic cell lines while the two metastatic cell lines also separated well (Fig. 1A).

Comparative analysis uncovered 177 phosphosites to be significantly altered (Student's Ttest, p-value<0.05) between two metastatic UM cell lines (OMM2.3 and OMM2.5) and the primary UM cell line Mel270 (Table 1).

Pathway analysis on the phosphosites upregulated in UM metastases revealed enrichment of Rho/Rac/Rnd GTPase signaling as well as mRNA splicing and cell cycle pathways (Table 2). GTPase activity is essential for the process of microtubule polymerisation during cell motility and division.

Pathway analysis on the downregulated phosphosites resulted in enrichment of the cascades responsible for immune response, such as interleukin signalling and virus antigen presentation (Table 3).

To link our phosphoproteome datasets to clinical endpoints in UM, we performed correlation analysis of the UM risk factor *BAP1* mRNA expression versus mRNA expression of Microtubule Affinity Regulating Kinase 1-4 (*MARK1-4*), reported upstream regulators of microtubule assembly [30]. We identified *MARK3* as having a weak but significant inverse correlation with mRNA expression of *BAP1* (Fig 1B). Reduction of BAP1 expression occurs due to inactivating mutations and monosomy on chromosome 3 during UM development, and it known to strongly increase metastatic potential. Hence, reverse correlation with *BAP1* mRNA expression means increased *MARK3* expression could be specific for metastases. Indeed, we found significant difference between *MARK3* expression in UM cases with different chromosome 3 status both in LUMC (Fig. 1C) and TCGA (Fig. 1E) patient cohorts. Moreover, in the LUMC cohort *MARK3* expression correlates with worse prognosis (Fig. 1D); in the TCGA cohort we observe a similar trend, but the difference is not significant. We did not find significant correlation between mRNA expression of *MARK1*, *2*, *4* and any of the tested clinical parameters (data not shown).

MARK3 is known to regulate Rho signaling (top pathway from phosphoproteomics) via ARGHEF2 [31]. Activated Rho/Rac1 are involved in many processes, including an indirect activation/nuclear translocation of transcriptional co-activators YAP1 and TAZ, suggesting a link between MARK3 and nuclear localization of YAP1/TAZ transcription factors via Rho signaling. Since nuclear localization of YAP1/TAZ have been found involved in proliferation of uveal melanoma cells, MARK3 might possibly be important for proliferation or invasion of UM cells.
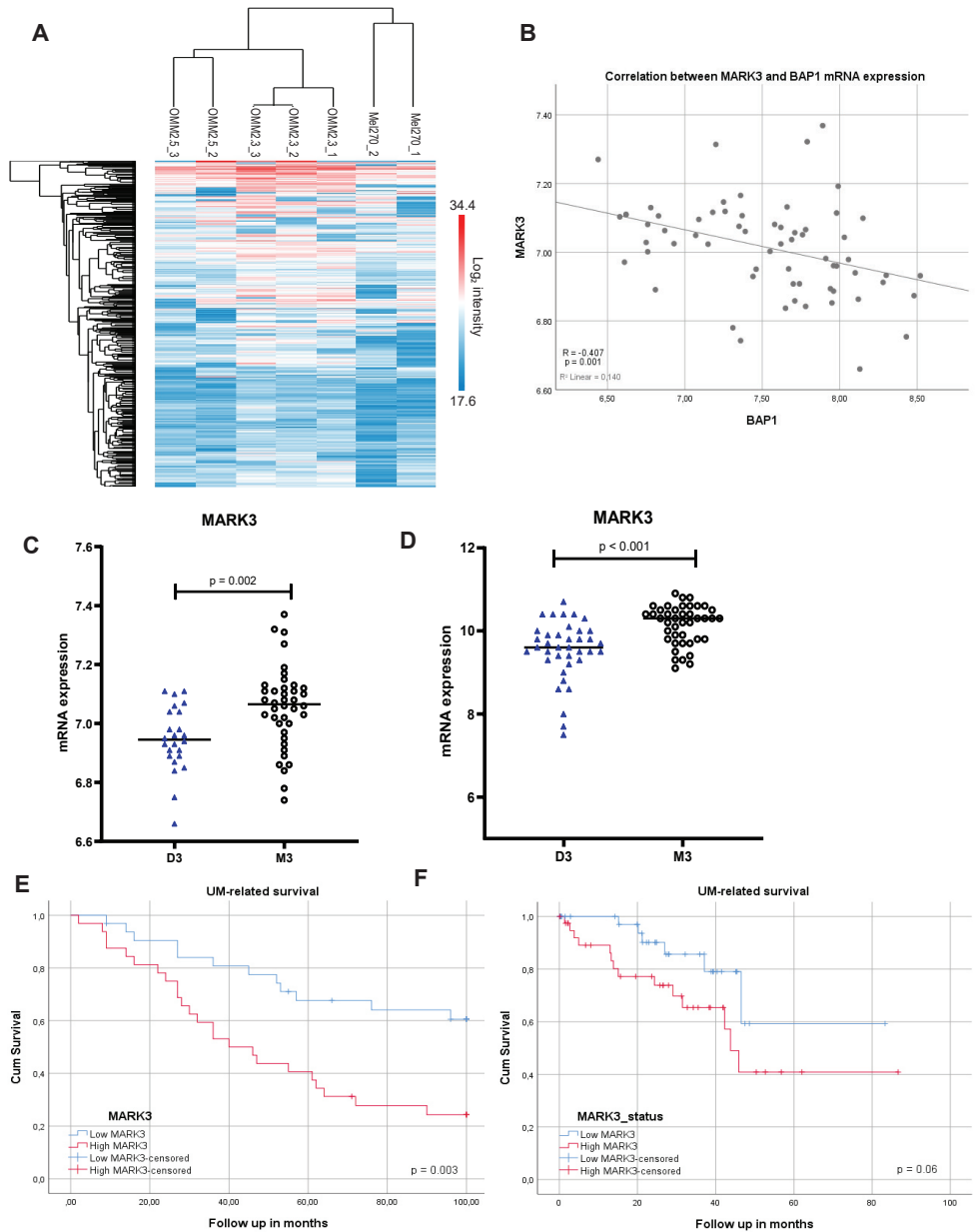
Figure 1. MARK3 expression correlates with the status of chromosome 3 and survival in UM.
(A) Heatmap of the phosphosites identified by mass-spectrometry analysis. (B) Correlation between MARK3 and BAP1 mRNA expression in LUMC cohort. (C-D) Correlation of MARK3 mRNA expression with chromosome 3 status of the tumors in (C) LUMC cohort, (D) TCGA cohort. (E-F) Analysis of the UM-specific survival related to MARK3 expression in (E) LUMC patient cohort (n=63; split at the median, n=32 high, n=31 low), (F) TCGA cohort, (n=71; split at the median, n=36 high, n=35 low).

Taken together, these results indicate potential significance of MARK3-Rho-YAP1/TAZ signaling axis for UM progression. Therefore, we decided to closely study the role of MARK3 on YAP1/TAZ signaling in context of UM.

Activity of MARK3 might interfere with YAP1/TAZ signaling

In order to evaluate the effect of MARK3 on UM cell viability, we generated MARK3-KO derivatives of UM cell lines MM66, OMM1, OMM2.3 and OMM2.5. In the case of MM66 and OMM2.5, we first introduced a Cas9 lentiviral expression vector and subsequently transduced MM66/Cas9 and OMM2.5/Cas9 with a lentivirus containing either control sgRNA (CR-NT) or sgRNAs targeting *MARK3* (CR-M3) (Suppl. Fig. 1A). In case of OMM1 and OMM2.3 we first stably expressed the MARK3-targeting sgRNAs and then transiently introduced Cas9 expressing adenoviral vector or a control vector (expressing GFP) (Suppl. Fig 1B). After generation of these polyclonal cell lines, we isolated monoclonal cell lines lacking MARK3 expression and used these monoclonal cell lines for further investigation. We treated these cell lines with the geranylgeranyl transferase inhibitor GGTI-298, a compound that indirectly attenuates YAP1/TAZ activity by inhibiting the activity of RhoA/Rac1 [32]. As illustrated in Fig. 2A and 2B, depletion of MARK3 in MM66 and OMM2.3 cells slightly reduced the level of TAZ compared to control cells and this effect is enhanced by GGTI-298 treatment. The level of YAP1, however, stays stable across all the conditions, although in OMM2.3 cells the band of YAP1 is migrating slightly slower upon GGTI-298 treatment, which might possibly indicate increased phosphorylation of YAP1. The same effect is illustrated on additional clones of OMM2.3 CR-M3 in Suppl. Fig. 2A. In OMM1 cells (Fig. 2B) the levels of both YAP1 and TAZ do not change upon MARK3 knockout and GGTI-298 treatment; in OMM2.5 CR-M3 clones TAZ levels are slightly downregulated upon GGTI-298 treatment comparing to vehicle treated samples (Suppl. Fig. 2B).

To determine whether MARK3 knockout has an effect on YAP1/TAZ activity, we investigated the expression of two classic YAP1/TAZ target genes *CTGF* (Fig. 2C and Suppl. Fig. 2C) and *CYR61* (Fig. 2D and Suppl. Fig. 2D), both basal and upon GGTI-298 treatment. The basal expression of *CTGF* was reduced in most MARK3 knockout cell lines compared to the controls, although not consistent in OMM2.5. The basal expression of *CYR61* is not significantly lower in most MARK3-KO cell lines, with exception in MM66 cells. In MM66 and OMM2.3 cell lines, treatment with GGTI-298 further downregulates expression of both YAP1/TAZ target genes, but OMM1 demonstrates no, or even the opposite effect. Again, the effects in OMM2.5 cells are not consistent.

Subsequently we investigated the consequence of MARK3 knock-out on cell viability upon GGTI-298 treatment. Interestingly, the combination of MARK3 knockout and GGTI-298 treatment synergistically inhibited growth of MM66, OMM2.3 and OMM2.5 cell lines, but not in the OMM1 cell lines (Fig. 2E and Suppl. Fig. E, F). This effect to some extent correlates with the effects of MARK3 knock-out on expression of the YAP1/TAZ target genes. It is important to note that MARK3 knockout did not consistently affect the growth rate of the UM cell lines (data not shown).
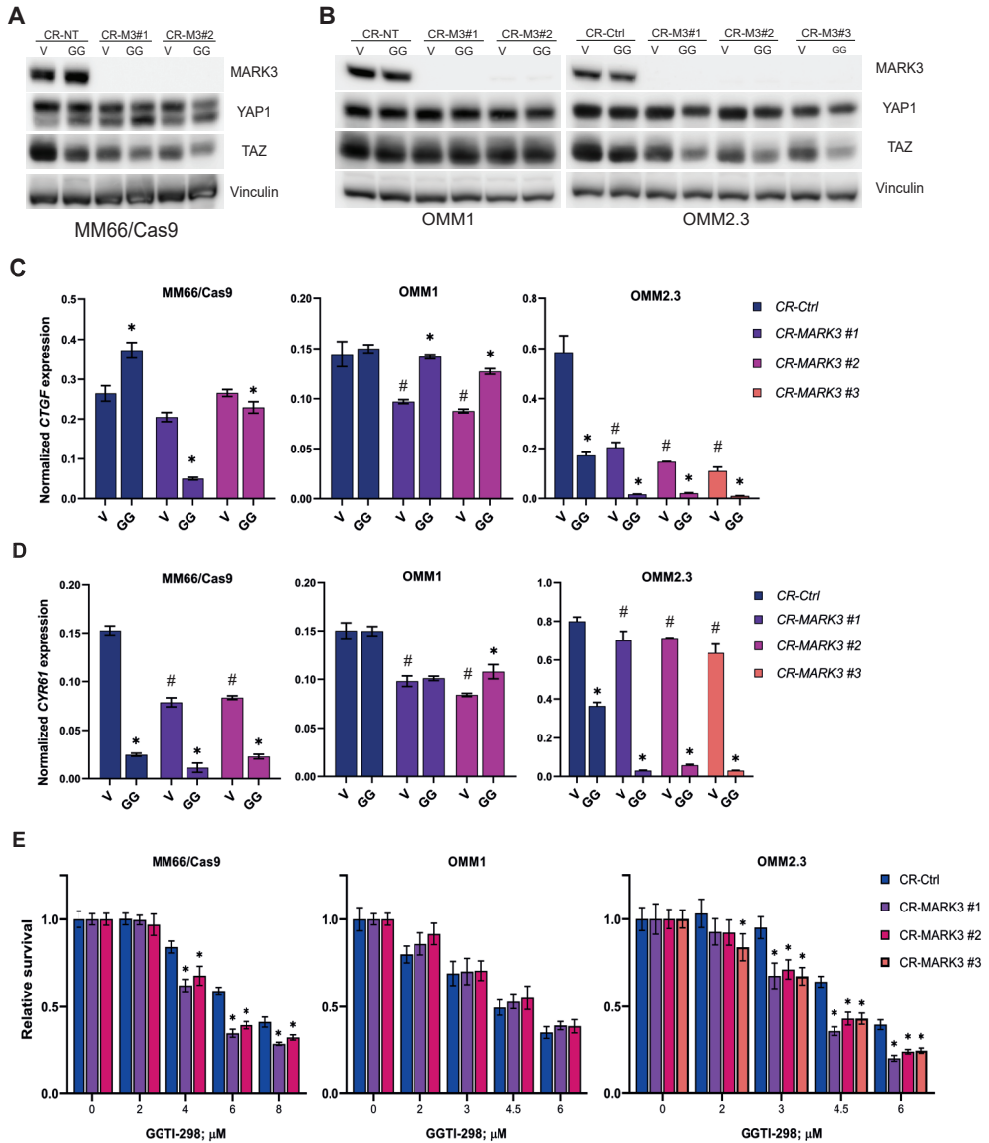
Figure 2. MARK3 knockout in combination with GGTI-298 synergistically inhibits growth of UM cell lines.
(A-B) Effect of MARK3 knockout on YAP1 and TAZ protein expression in (A) MM66, (B) OMM1 and OMM2.3.
V-vehicle, GG-GGTI-298 (6 µM for MM66 and OMM2.3, 4 µM for OMM1); Vinculin was used as a loading control.
(C-D) Expression of (C) *CTGF* and (D) *CYR61* mRNA upon 24h treatment with GGTI-298 in MARK3-knockout UM cell
lines. V-vehicle, GG-GGTI-298 (6 µM for MM66 and OMM2.3, 4 µM for OMM1); significant (p<0.05) change in mRNA
expression upon MARK3 knockout (CR-MARK3) compared to the vehicle CR-Ctrl is indicated with (#); significant
(p<0.05) change in mRNA expression upon GGTI-298 treatment compared to the vehicle control is indicated with (*),
statistical analysis was performed using one-way ANOVA, error bars present mean ± SEM, n=3. (E) Effect of GGTI-298
on viability of MARK3-knockout UM cell lines after 5 days of treatment. Significant (p<0.05) reduction of viability in
CR-MARK3 comparing to CR-Ctrl is indicated with (*), statistical analysis was performed using one-way ANOVA, error
bars present mean ± SEM, n=3.

Discussion

To detect signaling pathways, involved in UM metastatic spread, we compared phospho-proteomes of the cell lines derived from UM primary tumor and metastases. Mass spectrometry analysis indicated 177 differently phosphorylated sites, and some of the hits: ARHGEF2 [31], TNIK1 [33] HSF1 [34], SORBS2 [35], have been reported to participate in YAP1/TAZ signaling cascade. These results and our previous work (Chapter 4) indicate the involvement of YAP1/TAZ signaling in the process of UM metastatic spread.

In line with the studies of various cancer types [36], our pathway analysis indicated enrichment of GTPase activity related processes in metastatic cell lines compared to primary tumor. Specifically in UM, the elevated RhoC GTPase activity was reported in the tumors with higher metastatic potential harboring monosomy on chromosome 3 [37].

Interestingly, the down-regulated pathways in metastatic UM cell lines compared to a primary cell line are mostly related to immune response and antigen presentation. This effect has been described in metastatic UM and might be important for immune evasion [38].

MARK3 kinase has been shown to phosphorylate ARHGEF2 and thus stimulate activation of RhoA, which is an essential regulator of YAP1 activity in UM [12]. We demonstrate that full depletion of MARK3 expression results in down regulation of YAP1/TAZ target genes and, in case of MM66 and OMM2.3 cell lines affects the protein levels of TAZ. The inconsistent effect of MARK3 KO on mRNA expression of *CTGF* and *CYR61* in OMM2.5 might be attributed to possible off-target effects of sgRNAs, since the effects of GGTI-298 treatment is similar to the other cell lines. Moreover, we have previously shown (Chapter 4) that expression of *CYR61* in OMM2.5 is dependent on TAZ, but not YAP1.

In Chapter 4 we demonstrated that combination of YAP1/TAZ depletion with the geranyl-geranyl transferase inhibitor GGTI-298, acting downstream in the mevalonate pathway and reducing the activity of Rho proteins, synergistically slows down growth of UM cell lines. Similarly, when MARK3 knockout is combined with GGTI-298, the effect on transcription of YAP1/TAZ target genes is significantly enhanced, and the growth of some MARK3 KO UM cell lines is synergistically inhibited. However, the synergistic effect of the combination is not very strong and a proportion of the MARK3 KO cells remain viable even after prolonged incubation with relatively high concentrations of GGTI-298, what can indicate potential activation of resistant mechanisms.

The role of MARK3 in YAP1/TAZ signaling and tumor progression might be context dependent, as follows from the report of Machino et al., which showed that lower *MARK3* expression significantly correlated with poor prognosis in HGSOC patients [39]. This report is in contrast with our finding that high levels of *MARK3* correlates with worse prognosis of UM patients and that higher *MARK3* expression correlated with monosomy of chromosome 3. On the other hand, treatment of glioma cell lines with a recently described MARK3/MARK4 inhibitor reduced their proliferation *in vitro* and tumorigenic growth in a xenograft mouse model [40]. In UM we have not observed the consistent effect of MARK3 knockout on cell viability, and the combination of MARK3 knockout with GGTI-298 was not able to completely abrogate the growth of metastatic UM cell lines.

We conclude that MARK3 appears to be involved in YAP1/TAZ signaling regulation in UM, but its suitability as a therapeutic target needs further investigation.

Acknowledgements

Materials and Methods

Cell culture

Cell lines Mel270 (CVCL_C302), OMM2.5 (CVCL_C307), OMM2.3 (CVCL_C306) (a gift of Bruce Ksander) and OMM1 (CVCL_6939) were cultured in a mixture of RPMI and DMEM-F12 (1:1) supplemented with 10% FBS and antibiotics [23]. MM66 (CVCL_4D17) was cultured in IMDM supplemented with 20% FBS and antibiotics [24]. The cell lines were maintained in a humidified incubator at 37°C with 5% CO_2.

Mass-spectrometry analysis

Sample preparation

The experiments were performed according to the published protocol [25]. Briefly, the cells were collected by scraping in lysis buffer, then the lysates were heated to 95°C and cooled on ice, sonicated in a microtip sonicator, heated to 95°C and cooled on ice again. Subsequently, the proteins were precipitated with acetone overnight at -20°C. Protein precipitates were collected by centrifugation, washed with 80% acetone and air dried overnight.

Protein pellets were dissolved in digestion buffer and digested by 1% ProteaseMAX detergent (Promega, Madison, WI, USA) and Trypsin/Lys-C Mix (Promega, Madison, WI, USA) at a 1:50 ratio in a ThermoMixer C (Eppendorf, Nijmegen, The Netherlands) at 2,000 rpm for 18 hours at 37°C.

The digestion was stopped by adding 300 mM KCl, 5 mM KH_2PO_4, 50% ACN, 6% Trifluoroacetic acid (TFA), then phosphopeptides were enriched on TiO_2 beads. Phosphopeptides were eluted with 40% ACN, 15% NH_4OH, loaded onto StageTips packed with 3X layers of Empore SPE Disks SDB-RPS material (Sigma-Aldrich St Louis, MO, USA), washed with 0.2% TFA and eluted with 80% ACN, 5% NH_4OH. The eluates were lyophilized in a freezedryer and resuspended in 10 μl 0.1% Formic acid.

Mass spectrometry data acquisition

The experiments were performed on an EASY-nLC 1000 system (Proxeon, Odense, Denmark) connected to a Q-Exactive Orbitrap (Thermo Fisher Scientific, Germany) through a nanoelectrospray ion source. The Q-Exactive was coupled to a 35 cm analytical column with an inner-diameter of 75 μm, in-house packed with 1.9 μm C18-AQ beads (Reprospher-DE, Pur, Dr. Manish, Ammerbuch-Entringen, Germany) placed into a Butterfly Heater (Phoenix S&T, PA, USA) set to 50°C. The chromatography gradients were performed in 0.1% formic acid increasing the acetonitrile percentage gradually from 5% to 25% acetonitrile in 215 min, then to 30% in 15 min and up to 60% in the next 15 min followed by column re-equilibration. Flow rate was set at 250 nL/min. The mass spectrometer was operated in a Data-Dependent Acquisition (DDA) mode with a top-10 method and a scan range of 300-1600 m/z. Full-scan

5

MS spectra were acquired at a target value of 3 × 106 and a resolution of 70,000, and the Higher-Collisional Dissociation (HCD) tandem mass spectra (MS/MS) were recorded at a target value of 1 × 105 and with a resolution of 17,500, and isolation window of 2.2 m/z, and a normalized collision energy (NCE) of 25%. The minimum AGC target was 1x103. The maximum MS1 and MS2 injection times were 20 and 120 ms, respectively. The precursor ion masses of scanned ions were dynamically excluded (DE) from MS/MS analysis for 60 s. Ions with charge 1, and >6, were excluded from triggering MS2 analysis.

Mass spectrometry data analysis

Raw data were analyzed using MaxQuant (version 1.6.2.10) as described previously [26]. We performed the search against an in silico digested UniProt reference proteome for Homo sapiens including canonical and isoform sequences (18th June 2018). Database searches were performed according to standard settings with the following modifications. Oxidation (M), Acetyl (Protein N-term) and Phospho (STY) were allowed as variable modifications with a maximum number of 3. Label-Free Quantification was enabled, not allowing Fast LFQ. Match between runs was performed with 0.7 min match time window and 20 min alignment time window. All peptides were used for protein quantification. All tables were written. Phospho(STY)sites.txt file from the MaxQuant output was analysed in the Perseus computational platform (1.6.2.2) as described previously [27]. Phosphopeptide intensity values were log2 transformed and potential contaminants and proteins identified by site only or reverse peptide were removed. Phosphosites table was expanded into single, double, and multiple phosphosites and filtered to contain quantifications in at least one sample resulting in 14,315 quantified phosphosites. Samples without reasonable depth of sequencing/quality of data (Mel270 replicate 4, OMM2.3 replicate 4 and OMM2.3 replicates 1 and 4) or failed measurements (Mel270 replicate 3) were removed from the total datasets. This quality control step resulted in 13,600 phosphosites and were further subjected to stringent filtering (having intensities in 70% of the samples) resulting in 4,367 phosphosites in total. Missing values were imputed using normally distributed values with a 1.8 downshift (log2) and a randomized 0.3 width (log2) considering whole matrix values. Two-sided Student's T-tests with were performed between groups with a cut-off value of p=0.05. Statistical analysis tables were exported and processed in MS Excel, for further filtering and processing of the data. Phosphosites were marked significant when they pass the p-value cut-off during statistical analysis in both metastatic cell lines.

Generation of MARK3 knock-out cell lines

A Cas9-expressing lentivirus stock was produced by transfecting pKLV2-EF1a-Cas9Bsd-W (Addgene #68343) into HEK293T cells together with packaging vectors (psPax2 and pMD2.G). The MM66 and OMM2.5 cell lines were transduced with this lentivirus and were selected using Blasticidin S. These Cas9-expressing cell lines were subsequently transduced with lentiviruses either expressing a gRNA targeting MARK3 or a non-targeting gRNA, obtained from the human CRISPR Library (Sigma-Aldrich, St Louis, MO, USA). Transduced cells were selected with puromycin. To generate MARK3 KO cells we used two distinct gRNAs
(sequences: 5'-CACAGCTACATATTTGTTATTGG-3' (CR-MARK3#1) and
5'- TTTGACTATTTGGTTGCACATGG-3' (CR-MARK3#2).
Unfortunately, the CR-MARK3#1 gRNA was not efficient in generating a knock-out, and no monoclonal MARK3 KO cell lines could be generated with this gRNA. OMM2.3 and OMM1

cells were transduced with the same lentiviruses expressing MARK3-targeting gRNAs and selected with puromycin. Subsequently, these cell lines were transduced with adenovirus vectors expressing either GFP + Cas9, or only GFP as control, as we have described before [28].

As a control for efficiency of generation KO cell lines we used a lentivirus expressing a gRNA targeting the TP53 gene, described before [28].

Cell viability assay

The cells were seeded at their appropriate concentrations into clear 96-well plates. The next day, the medium was supplemented with GGTI-298. The treatment was repeated after 2 days. After 5 days from beginning of the experiment, the viability of the cells was assessed using the CellTiter-Blue cell viability assay (Promega, Madison, WI, USA).

Western blot

The cells were seeded into 6-well plates. Before harvesting, the cells were rinsed 2 times with ice-cold Phosphate Buffered Saline and scraped and lysed with Giordano buffer (50 mM Tris- HCl pH=7.4, 250 mM NaCl, 0.1% Triton X-100, 5 mM EDTA, supplemented with phosphatase and protease inhibitors. Equal protein amounts were separated on SDS-PAGE and blotted on PVDF membranes (Millipore, Darmstadt, Germany). The membranes were blocked with 10% non-fat dry milk in TBST buffer (10 mM Tris-HCl pH=8.0, 150 mM NaCl, 0.2% Tween-20) and incubated with the primary antibodies diluted in 5% bovine serum albumin/TBST overnight at 4 °C. The membranes were washed with TBST and incubated with horseradish peroxidaseconjugated secondary antibodies (Jackson Laboratories, Bar Harbor, ME, USA). The chemiluminescent signal was visualized using a Chemidoc machine (Biorad, Hercules, CA, USA).

Primary antibodies were obtained from Santa Cruz Biotechnology, Dallas, TX, USA; (MARK3 (F6) and p53 (DO-1), from Cell Signaling Technology, Beverly, MA, USA; (YAP1 (D8H1X) and TAZ (V386), from Sigma-Aldrich, St Louis, MO, USA; (Vinculin (V9131) and from Bethyl Laboratories, Montgomery, TX, USA (USP7; A300-033A).

RNA isolation and qPCR

The cells were seeded into 6-well plates. The next day, media were supplemented with GGTI- 298. After 3 days of treatment, cells were collected by scraping and placed in lysis buffer and RNA was isolated using the SV Total RNA Isolation System (Promega, Madison, WI, USA) according to the manufacturers' protocol. The reverse transcription reaction was performed using ImPromII reverse transcriptase (Promega). qPCR was performed using SYBR Green Mix (Roche Diagnostics, Indianapolis, IN, USA) in a C1000 Touch Thermal Cycler (Bio-Rad, Hercules, CA, USA). The relative expression of target genes was determined and corrected in relation to the housekeeping genes CAPNS1 and SRPR. In each experiment, the average relative expression was compared to the untreated. Primer sequences are listed in Supplementary Table 1.

Statistical analysis

The data were analyzed using GraphPad Prism software v.9.1.0 (GraphPad Software, San Diego, CA, USA). Student's t-test was used to analyze the difference between two groups. One-way ANOVA was used to analyze the differences between multiple groups. P values of

0.05 or less were considered significant.

Clinical data analysis

The LUMC cohort includes clinical, histopathological, and genetic information on 64 cases treated with primary enucleation at the Leiden University Medical Centre (LUMC) between 1999 and 2008. Clinical information was collected from the Integral Cancer Center West patient records and updated in 2021.

After enucleation, part of the tumor was snap frozen with 2-methyl butane and used for mRNA and DNA isolation, while the remainder was embedded in paraffin after 48 hours of fixation in 4% neutrally buffered formalin and was sent for histological analysis. RNA was isolated with the RNeasy mini kit (Qiagen, Venlo, The Netherlands) and mRNA expression was determined with the HT-12 v4 chip (Illumina, San Diego, CA, USA). Chromosome 3 status was obtained with Single-nucleotide polymorphism analysis, performed with the Affymetrix 250K_NSP-chip and Affymetrix Cytoscan HD chip (Affymetrix, Santa Clara, CA, USA). TCGA cohort represents 80 primary UM cases enucleated in 6 different centers. mRNA expression was determined by RNA-seq.

The statistical software SPSS, version 25 (IBM Corp, Armonk, NY, USA) was used for statistical analyses of the LUMC and TCGA cohorts. Survival analysis was performed with Kaplan-Meier and log-rank test, with death due to metastases as endpoint. Cases that died of another or unknown cause were censored. The two subpopulations that were compared in each analysis were determined by splitting the total cohort along the median value of mRNA expression for the analyzed gene.

The study was approved by the Biobank Committee of the Leiden University Medical Center (LUMC; 19.062.CBO/uveamelanoomlab-2019-3; B20.023). The tenets of the Declaration of Helsinki were followed.

References

1. Kim, J.H., S.J. Shin, S.J. Heo, E.A. Choe, C.G. Kim, M. Jung, et al. Prognoses and Clinical Outcomes of Primary and Recurrent Uveal Melanoma. Cancer Res Treat 2018; 50(4): 1238- 1251.

2. Kujala, E., T. Makitie,T. Kivela. Very long-term prognosis of patients with malignant uveal melanoma. Invest Ophthalmol Vis Sci 2003; 44(11): 4651-4659.

3. Olofsson, R., Cahlin, C., All-Ericsson, C. et al. Isolated Hepatic Perfusion for Ocular Melanoma Metastasis: Registry Data Suggests a Survival Benefit. Ann Surg Oncol 2014; 21, 466–472.

4. Nathan P, Hassel JC, Rutkowski P, Baurain JF, Butler MO, Schlaak M, et al. Overall Survival Benefit with Tebentafusp in Metastatic Uveal Melanoma. N Engl J Med 2021; 385(13):1196- 1206

5. Johansson, P., L.G. Aoude, K. Wadt, W.J. Glasson, S.K. Warrier, A.W. Hewitt, et al. Deep sequencing of uveal melanoma identifies a recurrent mutation in PLCB4. Oncotarget 2016; 7(4): 4624-4631.

6. Moore, A.R., E. Ceraudo, J.J. Sher, Y. Guan, A.N. Shoushtari, M.T. Chang, et al. Recurrent activating mutations of G-protein-coupled receptor CYSLTR2 in uveal melanoma. Nat Genet 2016; 48(6): 675-680.

7. Robertson, A.G., J. Shih, C. Yau, E.A. Gibb, J. Oba, K.L. Mungall, et al. Integrative Analysis Identifies Four Molecular and Clinical Subsets in Uveal Melanoma. Cancer Cell 2017; 32(2): 204-220 e15.

8. Chen, X., Q. Wu, P. Depeille, P. Chen, S. Thornton, H. Kalirai, et al. RasGRP3 Mediates MAPK Pathway Activation in GNAQ Mutant Uveal Melanoma. Cancer Cell 2017; 31(5): 685-696 e6.

9. Vaque, J.P., R.T. Dorsam, X. Feng, R. Iglesias-Bartolome, D.J. Forsthoefel, Q. Chen, et al. A genome-wide RNAi screen reveals a Trio-regulated Rho GTPase circuitry transducing mitogenic signals initiated by G protein-coupled receptors. Mol Cell 2013; 49(1): 94-108.

10. Wu, X., J. Li, M. Zhu, J.A. Fletcher,F.S. Hodi. Protein kinase C inhibitor AEB071 targets ocular melanoma harboring GNAQ mutations via effects on the PKC/Erk1/2 and PKC/NF-kappaB pathways. Mol Cancer Ther 2012; 11(9): 1905-1914.

11. Feng, X., N. Arang, D.C. Rigiracciolo, J.S. Lee, H. Yeerna, Z. Wang, et al. A Platform of Synthetic Lethal Gene Interaction Networks Reveals that the GNAQ Uveal Melanoma Oncogene Controls the Hippo Pathway through FAK. Cancer Cell 2019; 35(3): 457-472 e5.

12. Feng, X., M.S. Degese, R. Iglesias-Bartolome, J.P. Vaque, A.A. Molinolo, M. Rodrigues, et al. Hippo-independent activation of YAP by the GNAQ uveal melanoma oncogene through a trio-regulated rho GTPase signaling circuitry. Cancer Cell 2014; 25(6): 831-845.

13. Li, H., Q. Li, K. Dang, S. Ma, J.L. Cotton, S. Yang, et al. YAP/TAZ Activation Drives Uveal Melanoma Initiation and Progression. Cell Rep 2019; 29(10): 3200-3211 e4.

14. Vader, M.J.C., M.C. Madigan, M. Versluis, H.M. Suleiman, G. Gezgin, N.A. Gruis, et al. GNAQ and GNA11 mutations and downstream YAP activation in choroidal nevi. Br J Cancer 2017; 117(6): 884-887.

15. Decatur, C.L., E. Ong, N. Garg, H. Anbunathan, A.M. Bowcock, M.G. Field, et al. Driver Mutations in Uveal Melanoma: Associations With Gene Expression Profile and Patient Outcomes. JAMA Ophthalmol 2016; 134(7): 728-733.

16. Harbour, J.W., M.D. Onken, E.D. Roberson, S. Duan, L. Cao, L.A. Worley, et al. Frequent mutation of BAP1 in metastasizing uveal melanomas. Science 2010; 330(6009): 1410-1413.

17. Martin, M., L. Masshofer, P. Temming, S. Rahmann, C. Metz, N. Bornfeld, et al. Exome sequencing identifies recurrent somatic mutations in EIF1AX and SF3B1 in uveal melanoma with disomy 3. Nat Genet 2013; 45(8): 933-936.

18. Harbour, J.W. The genetics of uveal melanoma: an emerging framework for targeted therapy. Pigment Cell Melanoma Res 2012; 25(2): 171-181.

19. Kilic, E., W. van Gils, E. Lodder, H.B. Beverloo, M.E. van Til, C.M. Mooy, et al. Clinical and cytogenetic analyses in uveal melanoma. Invest Ophthalmol Vis Sci 2006; 47(9): 3703-7.

20. Shain, A.H., M.M. Bagger, R. Yu, D. Chang, S. Liu, S. Vemula, et al. The genetic evolution of metastatic uveal melanoma. Nat Genet 2019; 51(7): 1123-1130.

21. Ramasamy, P., C.C. Murphy, M. Clynes, N. Horgan, P. Moriarty, D. Tiernan, et al. Proteomics in uveal melanoma. Exp Eye Res 2014; 118: 1-12.

22. Zuidervaart, W., P.J. Hensbergen, M.C. Wong, A.M. Deelder, C.P. Tensen, M.J. Jager, et al. Proteomic analysis of uveal melanoma reveals novel potential markers involved in tumor progression. Invest Ophthalmol Vis Sci 2006; 47(3): 786-793.

23. Luyten, G.P., N.C. Naus, C.M. Mooy, A. Hagemeijer, J. Kan-Mitchell, E. Van Drunen, et al. Establishment and characterization of primary and metastatic uveal melanoma cell lines. Int J Cancer 1996; 66(3): 380-387.

24. Amirouchene-Angelozzi, N., F. Nemati, D. Gentien, A. Nicolas, A. Dumont, G. Carita, et al. Establishment of novel cell lines recapitulating the genetic landscape of uveal melanoma and preclinical validation of mTOR as a therapeutic target. Mol Oncol 2014; 8(8): 1508-1520.

25. Sampadi B, Mullenders LHF, Vrieling H. Phosphoproteomics Sample Preparation Impacts Biological Interpretation of Phosphorylation Signaling Outcomes. Cells 2021; 10(12):3407

26. Tyanova S, Temu T, Cox J. The MaxQuant computational platform for mass spectrometrybased shotgun proteomics. Nat Protoc 2016; 11(12):2301-2319.

27. Tyanova, S., Temu, T., Sinitcyn, P. et al. The Perseus computational platform for comprehensive analysis of (prote)omics data. Nat Methods 2016; 13: 731–740.

28. Heijkants, R.C., A. Teunisse, D. de Jong, K. Glinkina, H. Mei, S.M. Kielbasa, et al. MDMX Regulates Transcriptional Activity of p53 and FOXO Proteins to Stimulate Proliferation of Melanoma Cells. Cancers (Basel) 2022; 14(18).

29. White, J.S., R.L. Becker, I.W. McLean, A.E. Director-Myska,J. Nath. Molecular cytogenetic evaluation of 10 uveal melanoma cell lines. Cancer Genet Cytogenet 2006; 168(1): 11-21.

30. Drewes G, Ebneth A, Preuss U, Mandelkow EM, Mandelkow E. MARK, a novel family of protein kinases that phosphorylate microtubule-associated proteins and trigger microtubule
disruption. Cell 1997; 89(2):297-308

31. Sandi, M.J., C.B. Marshall, M. Balan, E. Coyaud, M. Zhou, D.M. Monson, et al. MARK3- mediated phosphorylation

of ARHGEF2 couples microtubules to the actin cytoskeleton to establish cell polarity. Sci Signal 2017; 10(503).

32. Sorrentino, G., N. Ruggeri, V. Specchia, M. Cordenonsi, M. Mano, S. Dupont, et al. Metabolic control of YAP and TAZ by the mevalonate pathway. Nat Cell Biol 2014; 16(4): 357-66.

33. Pagliari, S., Vinarsky, V., Martino, F. et al. YAP–TEAD1 control of cytoskeleton dynamics and intracellular tension guides human pluripotent stem cell mesoderm specification. Cell Death Differ 2021; 28: 1193–1207.

34. Ferrari, N., R. Ranftl, I. Chicherova, N.D. Slaven, E. Moeendarbary, A.J. Farrugia, et al. Dickkopf-3 links HSF1 and YAP/TAZ signalling to control aggressive behaviours in cancerassociated fibroblasts. Nat Commun 2019; 10(1): 130.

35. Kuroda, M., K. Ueda,N. Kioka. Vinexin family (SORBS) proteins regulate mechanotransduction in mesenchymal stem cells. Sci Rep 2018; 8(1): 11581.

36. Fife CM, McCarroll JA, Kavallaris M. Movers and shakers: cell cytoskeleton in cancer metastasis. Br J Pharmacol 2014; 171(24): 5507-5523

37. Tura A, Lueke M, Reinsberg M, Ranjbar M, Kraus A, Grisanti S, Lueke J. Elevated RhoC expression and Rho-kinase activity in the uveal melanoma cells with Monosomy-3. Invest Ophthalmol Vis Sci 2006; 57: 5903.

38. Jager, M.J., Shields, C.L., Cebulla, C.M. et al. Uveal melanoma. Nat Rev Dis Primers 2020; 6: 24.

39. Machino, H., S. Kaneko, M. Komatsu, N. Ikawa, K. Asada, R. Nakato, et al. The metabolic stress-activated checkpoint LKB1-MARK3 axis acts as a tumor suppressor in high-grade serous ovarian carcinoma. Commun Biol 2022; 5(1): 39.

40. Li, F., Z. Liu, H. Sun, C. Li, W. Wang, L. Ye, et al. PCC0208017, a novel small-molecule inhibitor of MARK3/MARK4, suppresses glioma progression in vitro and in vivo. Acta Pharm Sin B 2020; 10(2): 289-300.

Supplementary figures
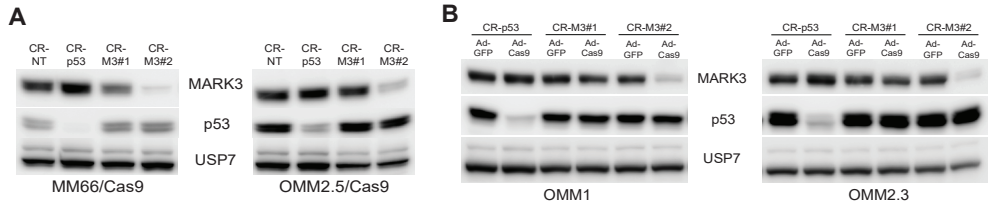
Supplementary Figure 1. MARK3 knockout derivatives of UM cell lines (A) MM66 and OMM2.5 cell lines were transduced with a lentiviral vector expressing Cas9 and subsequently transduced with a lentivirus containing either control sgRNA (CR-NT) or sgRNAs targeting MARK3 (CR-M3). **(B)** OMM1 and OMM2.3 were transduced with a lentiviral vector expressing MARK3-targeting sgRNAs (CR-M3) and then transiently introduced Cas9 expressing adenoviral vector or a control vector (expressing GFP). sgRNA targeting p53 (CR-p53) was used as a positive control for Cas9 activity, USP7 -loading control.

5
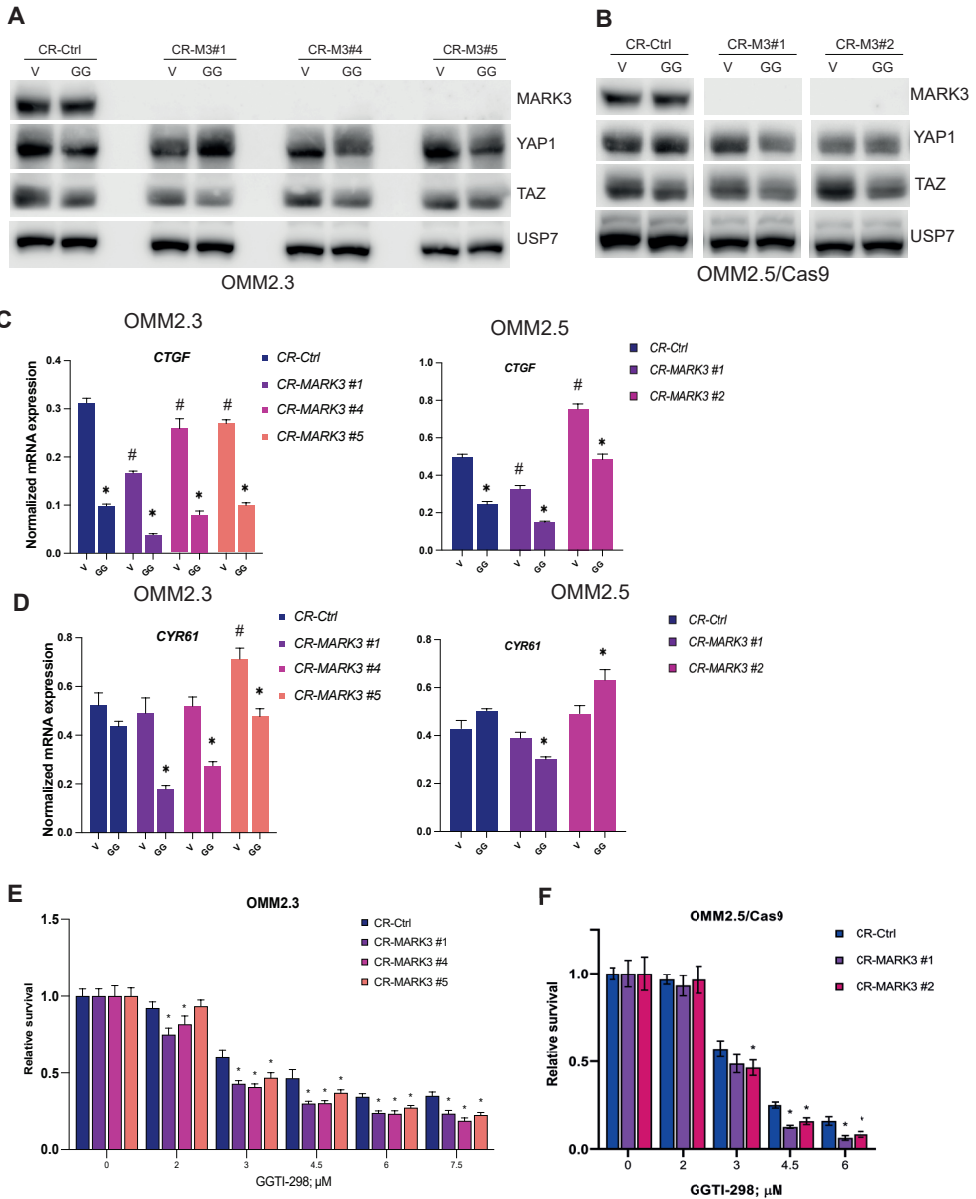
Supplementary Figure 2. Effect of MARK3 knockout on YAP1/TAZ signaling

(A-B) Effect of MARK3 knockout on YAP1 and TAZ protein expression in (A) OMM2.3, (B) OMM2.5. V-vehicle, GG-GGTI-298 (6 μM), CR-Ctrl - Non-targeting control, CR-M3 - MARK3 knockout ; USP7 was used as a loading control. (C-D) Expression of (C) CTGF and (D) CYR61 mRNA upon 24h treatment with GGTI-298 in MARK3-depleted UM cell lines. V-vehicle, GG-GGTI-298 (6 μM); significant (p<0.05) change in mRNA expression upon MARK3 knockout (CR-MARK3) compared to the vehicle control (CR-Ctrl) is indicated with (#); significant (p<0.05) change in mRNA expression upon GGTI-298 treatment compared to the vehicle control is indicated with (*), statistical analysis was performed using one-way ANOVA, error bars present mean ± SEM, n=3. (E) Effect of GGTI-298 on viability of MARK3-depleted UM cell lines after 5 days of treatment. Significant (p<0.05) reduction of viability in MARK3 knockout (CR-MARK3) comparing to control (CR-Ctrl) is indicated with (*), statistical analysis was performed using one-way ANOVA, error bars present mean ± SEM, n=3.

Tables

Table 1. Phosphosites significantly altered (Student's T-test, p-value<0.05) between two metastatic UM cell lines (OMM2.3 and OMM2.5) and the primary UM cell line Mel270.

Gene names_Amino acid Position_Multiplicity	Gene name	-Log Student's T-test p-value omm2.3_mel270	Log2 (omm2.3/mel270)	-Log Student's T-test p-value omm2.5_mel270	Log2 (omm2.5/mel270)
PNN_S100___1	PNN	2,320331	8,640889	2,326058	8,241045
ERBB2IP_S932___2	ERBB2IP	2,268686	8,470394	2,958135	7,317758
RASAL2_S877___2	RASAL2	3,20149	8,333005	2,054684	6,952386
SRRM2_S1404___2	SRRM2	2,692575	8,224896	1,868759	6,993231
ESCO2_S75___1	ESCO2	2,562178	8,201956	1,522422	6,608265
RASAL2_S880___2	RASAL2	3,90723	8,101601	2,888066	6,720983
CHD1_S1688___1	CHD1	2,308205	8,066828	2,482959	7,221378
TJP1_S605___1	TJP1	3,180118	7,891733	1,787064	6,33797
RRAGC_S95___1	RRAGC	3,014953	7,501115	1,379549	6,178071
SPAG9_S194___2	SPAG9	2,425856	7,390155	1,898788	5,164712
XRCC1_T226___2	XRCC1	2,875986	7,348891	2,017536	6,077906
SPAG9_S183___2	SPAG9	3,316868	7,330834	2,17075	6,32826
AHNAK_S5739___1	AHNAK	2,524264	7,191865	1,805079	5,962292
LARP1_S90___1	LARP1	2,601892	7,160233	1,872783	6,213362
TMPO_T208___1	TMPO	2,896412	7,094262	2,272455	5,42924
GPHN_S127___2	GPHN	2,161983	6,929839	1,471395	5,604192
SPAG9_S185___2	SPAG9	2,140266	6,712272	3,452904	6,417998
HSF1_S363___1	HSF1	2,696823	6,705507	2,782979	5,556595
TNS3_S420___1	TNS3	2,589706	6,695664	1,526324	5,546488
FAM83H_S250___1	FAM83H	2,496251	6,673758	1,92563	4,863586
PRR12_T1561___2	PRR12	2,581235	6,643726	1,593389	5,458888
PDE4D_S59___2	PDE4D	2,479143	6,605954	1,3098	5,063583
TNIK_S740___1	TNIK	3,612384	6,356614	2,168933	4,661845
JPH1_S220___2	JPH1	3,185261	6,329502	2,421806	5,579263
EPB41L2_S613___1	EPB41L2	3,686437	6,281228	3,121418	4,778723
RCOR1_S460___1	RCOR1	1,846028	6,255202	2,562084	5,780265
ATXN2_S679___2	ATXN2	1,810305	6,198335	1,753906	5,561078
CDK13_T871___1	CDK13	2,538078	6,131416	2,029476	4,644557
EPB41L2_S612___1	EPB41L2	2,768466	6,127415	1,689263	4,62491
GTSE1_S575___2	GTSE1	2,643891	6,125573	2,009009	4,778836
XRCC1_S235___2	XRCC1	2,655986	6,120244	1,842754	4,849258
CTNND1_S252___1	CTNND1	2,05667	6,113639	1,788081	4,697748
MKI67_T1991___2	MKI67	2,556213	6,1061	1,366884	4,969499
ACTR8_S166___1	ACTR8	2,963651	6,054322	2,627399	5,035097
ZNF318_S1243___1	ZNF318	2,231534	6,054263	2,051044	4,478581
HIRIP3_S370___1	HIRIP3	3,954943	6,001266	2,222852	5,618008
PRR12_S1568___2	PRR12	2,415128	5,971622	1,460491	4,786783
SPAG9_T191___2	SPAG9	2,536629	5,963344	1,720939	4,602517
PRKD1_S548___1	PRKD1	3,116462	5,962165	2,27624	4,249267
TOE1_S5___1	TOE1	1,753938	5,954744	1,716579	4,808053
EGLN1_S125___1	EGLN1	2,857895	5,919385	1,796896	4,478971
JPH1_T448___2	JPH1	2,798863	5,902094	1,90509	4,473262
GTSE1_S580___2	GTSE1	2,505914	5,865825	1,807325	4,519089
MAP3K3_S166___1	MAP3K3	2,312343	5,858965	1,834668	4,289849
TMEM106B_S33___1	TMEM106B	3,000869	5,754457	1,415835	3,974044
TCF3_S101___1	TCF3	2,488973	5,733511	1,591653	4,109531
BUB1_S593___2	BUB1	3,375849	5,717204	1,829598	3,570386
MDC1_S485___1	MDC1	2,666944	5,679147	2,418456	4,41726
DST_S2919___1	DST	2,806226	5,663026	1,645212	5,231556
TJP1_S912___1	TJP1	1,927121	5,640709	2,090857	4,063324

Table 1. (continued)

STUB1_S23___1	STUB1	2,189052	5,633894	1,378019	3,962584
TNKS1BP1_S1666___1	TNKS1BP1	2,231932	5,562864	1,416567	3,900805
SORBS2_S344___2	SORBS2	2,422821	5,492752	1,362648	4,325774
SORBS2_S346___2	SORBS2	2,422821	5,492752	1,362648	4,325774
BRSK1_S511___1	BRSK1	3,037206	5,472331	1,64215	3,743617
MTM1_S18___1	MTM1	2,4744	5,376583	1,499966	4,001469
JPH1_S452___2	JPH1	2,422273	5,364996	1,504618	3,936164
OSBPL3_S304___1	OSBPL3	2,66361	5,353166	1,493494	3,876441
WRNIP1_S75___1	WRNIP1	2,351422	5,338128	2,505737	3,776667
ZNF318_S1856___1	ZNF318	2,836324	5,300036	1,848118	3,729122
CTTN_S417___2	CTTN	2,637005	5,284897	1,829708	3,859484
HIRA_S610___2	HIRA	2,44548	5,27123	1,775098	3,811494
PDE4D_S284___1	PDE4D	3,176871	5,227415	1,305763	3,549265
KIF21A_S1199___1	KIF21A	2,600429	5,211912	1,464811	3,144364
ACIN1_S352___2	ACIN1	2,214204	5,152445	1,990831	3,309524
CAMSAP2_S1121___1	CAMSAP2	1,889824	5,150283	1,699402	3,913262
TCOF1_S171___2	TCOF1	2,133965	5,12712	1,559842	3,779662
PPFIBP1_S447___3	PPFIBP1	2,7788	5,096501	1,431068	2,931659
MAP2_S1782___1	MAP2	1,956307	5,068739	1,442695	4,316577
PRKD1_S549___1	PRKD1	2,500695	5,062782	1,490412	3,349884
TNKS1BP1_S1024___1	TNKS1BP1	3,031735	5,020459	1,38034	3,339321
KIF20A_S514___1	KIF20A	2,346576	5,014309	1,374915	3,525265
KIAA0195_S467___1	KIAA0195	2,011465	4,972063	1,305692	4,59376
MAPKBP1_S1075___1	MAPKBP1	2,238285	4,905191	1,485241	3,328155
BAIAP2L2_S451___1	BAIAP2L2	2,981735	4,729639	1,724977	2,91421
HIRA_S612___2	HIRA	2,575035	4,71989	3,71532	3,260154
TFIP11_S98___1	TFIP11	1,966688	4,70675	1,759056	3,459704
JPH1_S216___2	JPH1	2,966486	4,68522	2,547877	3,93498
FAM208A_S979___2	FAM208A	1,917645	4,678004	1,429208	3,537229
HELZ_S1615___1	HELZ	2,910573	4,664665	2,200548	3,688425
LIMA1_S362___1	LIMA1	2,481092	4,657305	1,918401	3,343395
ZNF576_S23___1	ZNF576	2,312478	4,641251	1,581668	3,39615
NAV3_S1190___2	NAV3	1,526135	4,618491	1,728742	3,589816
GTF2I_Y79___1	GTF2I	2,861768	4,607582	1,905497	3,825706
INTS10_S28___1	INTS10	1,909621	4,539656	2,033319	3,565192
NAV3_S1189___2	NAV3	1,50071	4,486849	1,755137	3,458174
VCL_S346___1	VCL	2,489016	4,439525	1,456603	4,23619
LZTS1_S50___1	LZTS1	1,645176	4,439265	1,797248	2,975595
SORBS2_S417___1	SORBS2	3,192156	4,407377	1,866019	3,067004
ARHGEF11_T1461___2	ARHGEF11	1,333038	4,393947	1,854821	3,925725
TRMT10A_S318___1	TRMT10A	2,806635	4,352537	2,80137	3,023454
NME1-NME2_S265___1	NME1-NME2	1,843706	4,339633	1,855448	2,425934
SCRIB_T475___1	SCRIB	1,883833	4,302811	1,389351	3,092653
TCP1_S320___1	TCP1	1,869216	4,27508	1,846498	3,023278
MYO5A_S600___1	MYO5A	2,281053	4,244164	1,803709	2,702554
MAPT_S232___1	MAPT	2,861958	4,219584	1,52609	3,139043
KIAA1109_S4612___1	KIAA1109	2,406284	4,175565	1,415593	2,338774
SPEN_S1278___1	SPEN	1,500086	4,132838	1,732827	2,879772
MAP7D1_S86___1	MAP7D1	1,478594	4,109335	2,190579	3,461679
ARHGAP31_S346___1	ARHGAP31	2,44578	4,100852	1,669664	3,386358
ARHGEF7_S516___1	ARHGEF7	2,083972	4,086313	2,045758	2,61045
INCENP_S312___3	INCENP	2,38039	4,053528	1,43104	3,280114

Table 1. (continued)

SNTB1_S389___1	SNTB1	2,198672	4,034518	1,325791	3,046955
DIP2B_S100___1	DIP2B	2,109784	4,023792	1,885077	3,181891
NSUN2_S357___1	NSUN2	2,351218	4,018664	1,329648	2,510872
NAV1_S819___1	NAV1	2,942902	3,995465	1,908395	2,495599
RICTOR_S1388___2	RICTOR	1,581062	3,986675	1,755504	2,533193
PTPN1_S50___1	PTPN1	1,955495	3,978933	4,128371	1,813383
BAZ1B_S347___1	BAZ1B	2,427764	3,967728	1,522676	2,284177
PPFIBP2_S67___1	PPFIBP2	3,112321	3,961967	1,509483	2,271859
CGN_S149___1	CGN	2,675491	3,873994	1,801435	2,347765
TCOF1_S906___1	TCOF1	2,888918	3,870422	1,760603	2,50899
MLIP_T135___2	MLIP	2,28447	3,836281	1,682248	2,40477
MON1A_S64___1	MON1A	2,242929	3,767194	2,112221	1,978688
AHNAK_S5752___1	AHNAK	2,225449	3,693034	2,11725	2,551395
ARHGEF2_S196___1	ARHGEF2	3,18585	3,648309	2,775792	-3,05644
SIPA1L2_S1488___1	SIPA1L2	2,586717	3,590309	1,923113	1,891082
FOXM1_T711___2	FOXM1	1,988807	3,548108	1,355429	1,59677
CDC25C_S55___2	CDC25C	3,076168	3,491254	1,934797	3,041707
LARP7_T344___2	LARP7	1,336955	3,478319	2,431372	1,761458
TJP1_S1487___1	TJP1	2,801101	3,466013	2,579193	2,454255
PHIP_S1783___1	PHIP	3,276471	3,46228	1,459985	1,706525
EMD_S173___1	EMD	1,70478	3,43758	1,322032	-4,77058
ZBTB21_S411___1	ZBTB21	3,425467	3,42332	2,588625	2,249149
HSF1_S303___1	HSF1	1,361852	3,41929	1,711162	2,243472
ANLN_S517___2	ANLN	2,246515	3,417024	2,048682	2,798349
ANXA2_S12___1	ANXA2	1,992307	3,409278	1,351751	2,456995
ZNF608_S964___1	ZNF608	1,847191	3,388404	1,854577	3,188241
KIF16B_S662___1	KIF16B	1,382869	3,321535	1,810152	1,745818
HMGXB4_S497___1	HMGXB4	2,104139	3,319221	1,948051	1,847479
CASC3_S117___1	CASC3	2,270714	3,309143	1,646314	1,941312
MICALL1_S484___2	MICALL1	1,884212	3,302014	1,389907	1,881289
MICALL1_S486___2	MICALL1	1,884212	3,302014	1,389907	1,881289
CDC25B_S375___1	CDC25B	1,354262	3,299366	3,547596	2,638251
ILK_S217___1	ILK	1,43567	3,250893	2,025503	1,501854
TNIK_S571___1	TNIK	3,051548	3,249062	1,656601	1,935293
HDAC1_S409___1	HDAC1	1,626491	3,246864	1,562885	1,975478
FMN1_S530___1	FMN1	1,51648	3,19901	1,736315	1,576665
TRIOBP_S171___1	TRIOBP	1,541126	3,168416	1,873288	0,765635
INCENP_S314___3	INCENP	2,324095	3,160938	1,361574	2,387524
NAV1_S103___1	NAV1	1,728778	3,061455	1,801629	1,523159
AHNAK_S5763___1	AHNAK	1,985461	3,023725	1,697325	-3,41666
DNMT3A_S75___1	DNMT3A	1,881033	3,001957	1,305662	2,096782
LIG1_T182___1	LIG1	2,6195	2,987185	1,575949	2,085989
MAPT_S552___2	MAPT	1,948161	2,863329	2,701347	1,753795
MAPT_T548___2	MAPT	1,948161	2,863329	2,701347	1,753795
COBLL1_T315___2	COBLL1	1,56267	2,858164	1,591365	1,213923
AP3B1_S227___1	AP3B1	1,48636	2,698777	1,639431	1,325895
CCNL1_S335___2	CCNL1	1,692334	2,683365	1,933779	-7,1822
EIF4G1_S1046___1	EIF4G1	2,69681	2,662518	3,280758	2,165616
IRS1_S348___1	IRS1	1,385602	2,63518	1,896005	2,087225
BACE2_S415___2	BACE2	1,661837	2,620349	1,514606	1,132684
LATS1_S181___1	LATS1	1,772975	2,57788	1,394203	0,904054
PRKD1_S205___2	PRKD1	1,395023	2,359995	1,703735	1,252979

5

Table 1. (continued)

PRKD1_S208___2	PRKD1	1,395023	2,359995	1,703735	1,252979
RNF169_T410___3	RNF169	1,414928	2,284362	1,319031	1,194876
SSBP3_T250___1	SSBP3	1,66804	2,240761	2,252237	1,39275
SLC1A5_S317___1	SLC1A5	1,582213	2,220436	2,874208	1,029798
OSBPL3_S309___2	OSBPL3	1,360713	2,060791	1,393556	0,767565
MON2_S205___1	MON2	1,42528	1,89273	1,726918	-3,57144
SCRIB_S1220___1	SCRIB	1,83174	1,860787	1,743541	0,940604
ZNF106_S1370___1	ZNF106	1,673556	1,832644	2,062451	-3,97011
SRGAP1_S936___2	SRGAP1	1,840648	1,743917	2,510153	-2,34698
TOP2A_S1391___2	TOP2A	1,440786	1,690183	3,755418	-4,8608
TOP2A_S1392___2	TOP2A	1,440786	1,690183	1,37965	0,681154
TOP2A_S1393___2	TOP2A	1,440786	1,690183	1,37965	0,681154
PDE4DIP_S903___1	PDE4DIP	2,113536	1,66637	1,667979	-0,68882
PDE4DIP_T904___1	PDE4DIP	2,113536	1,66637	1,475524	-0,7219
PHACTR4_S254___2	PHACTR4	2,655822	1,474211	1,517245	0,584294
PHACTR4_S275___2	PHACTR4	2,655822	1,474211	1,517245	0,584294
MYCBP2_S2749___2	MYCBP2	1,817208	0,846	2,122912	-0,50602
MYCBP2_S2751___2	MYCBP2	1,817208	0,846	2,122912	-0,50602
TACC2_S56___2	TACC2	2,101844	-2,3101	1,35654	-3,06379
TACC2_S60___2	TACC2	2,101844	-2,3101	1,35654	-3,06379
CANX_S475___1	CANX	1,827609	-4,90162	2,046562	-6,52963

Table 2. Pathway analysis on the phosphosites upregulated in UM metastases.

Pathway name	Entities FDR
Signaling by Rho GTPases	2,49E-09
Signaling by Rho GTPases, Miro GTPases and RHOBTB3	3,16E-09
RHO GTPase cycle	2,59E-07
Cell Cycle	2,12E-04
Cell Cycle, Mitotic	5,15E-04
Insulin-like Growth Factor-2 mRNA Binding Proteins (IGF2BPs/IMPs/VICKZs) bind RNA	1,16E-03
Apoptotic execution phase	2,89E-03
Apoptotic cleavage of cellular proteins	7,21E-03
Cell Cycle Checkpoints	1,06E-02
SUMO E3 ligases SUMOylate target proteins	1,87E-02
RHO GTPases Activate Formins	1,87E-02
RHOJ GTPase cycle	1,87E-02
RHOA GTPase cycle	2,19E-02
SUMOylation	2,19E-02
RHOQ GTPase cycle	2,19E-02
Mitotic Anaphase	2,19E-02
Mitotic Metaphase and Anaphase	2,19E-02
Amplification of signal from the kinetochores	2,19E-02
Amplification of signal from unattached kinetochores via a MAD2 inhibitory signal	2,19E-02
RHOC GTPase cycle	2,19E-02
M Phase	2,19E-02
RAC3 GTPase cycle	3,23E-02
RND3 GTPase cycle	3,23E-02
Unwinding of DNA	3,23E-02
RND2 GTPase cycle	3,23E-02
RHOU GTPase cycle	3,23E-02
MECP2 regulates neuronal receptors and channels	3,23E-02
mRNA Splicing - Major Pathway	3,71E-02
Metabolism of RNA	3,71E-02
RHOB GTPase cycle	3,83E-02
CDC42 GTPase cycle	3,83E-02
Depolymerization of the Nuclear Lamina	3,95E-02
RAC2 GTPase cycle	4,05E-02
RHOG GTPase cycle	4,56E-02
Mitotic Spindle Checkpoint	4,59E-02
RHO GTPase Effectors	4,81E-02
mRNA Splicing	4,86E-02

5

Table 3. Pathway analysis on the phosphosites downregulated in UM metastases.

Pathway name	Entities FDR
Maturation of spike protein	1,03E-02
Assembly of Viral Components at the Budding Site	1,03E-02
Interleukin-27 signaling	1,03E-02
Virus Assembly and Release	1,03E-02
Interleukin-35 Signalling	1,03E-02
Calnexin/calreticulin cycle	1,31E-02
Antigen Presentation: Folding, assembly and peptide loading of class I MHC	1,31E-02
Translation of Structural Proteins	1,31E-02
N-glycan trimming in the ER and Calnexin/Calreticulin cycle	1,31E-02
Maturation of spike protein	1,31E-02
Interleukin-12 family signaling	1,93E-02
Translation of Structural Proteins	2,13E-02
Late SARS-CoV-2 Infection Events	2,64E-02
MHC class II antigen presentation	2,64E-02
SARS-CoV-1 Infection	2,64E-02
Influenza Infection	2,94E-02

Supplementary tables

Supplementary Table 1. Primers for qPCR.

Primer	Sequence
CAPNS1 FW	ATGGTTTTGGCATTGACACATG
CAPNS1 RV	GCTTGCCTGTGGTGTCGC
CTGF FW	GTTTGGCCCAGACCCAACTA
CTGF FW	GGCTCTGCTTCTCTAGCCTG
CYR61 FW	CAGGACTGTGAAGATGCGGT
CYR61 RV	GCCTGTAGAAGGGAAACGCT
SRPR FW	CATTGCTTTTGCACGTAACCAA
SRPR RV	ATTGTCTTGCATGCGGCC

5